JOURNAL OF PROPULSION AND POWER
Vol. 12, No. 1, January–February 1996

Role of Slip in the Generation of Acoustic Instabilities in Gas Turbines

M. DiCicco*
University of Illinois at Urbana–Champaign, Urbana, Illinois 61801
and
J. Buckmaster†
Hong Kong University of Science and Technology, Kowloon, Hong Kong

Slip affects the response time of fuel sprays to acoustic fluctuations in a gaseous flowfield. This article describes how gaseous fuel is released by evaporation as an oscillating response to the acoustic velocity fluctuations, and so contributes to acoustic instability. This article discusses the differences due to the evaporation characteristics of various fuels (JP-4, JP-5, and D-2) as well as the effect of droplet size, inlet air temperature, air speed, and Reynolds number on mass response. For example, it is shown that instability will be driven harder at lower frequencies, higher gas velocities, and increased liquid volatility.

Nomenclature

C_D = coefficient of drag
C_p = specific heat at constant pressure, kJ/kg-K
c = speed of sound, m/s
FAR = fuel/air ratio
f = droplet evaporation rate per unit volume, kg/s
k = thermal conductivity, kW/m-K
L = latent heat of vaporization, kJ/kg
M = Mach number
MFR = fuel/air mass flux ratio
P = pressure, kPa
Pr = Prandtl number
Re_d = Reynolds number based on drop diameter
r = droplet radius, m
SMD = Sauter mean diameter, m
s = strained distance, m
s_e = strained droplet evaporation distance, m
T = temperature, K
t = time, s
U = steady-state freestream velocity, m/s
u = velocity, m/s
u_r = relative velocity between liquid droplets and air, m/s
W = density at given temperature, kg/m^3
x = distance, m
x_e = droplet evaporation distance, m
x_1 = stretching variable, m
Y = mass fraction
ε = asymptotic expansion parameter
μ = dynamic viscosity, kg/m-s
ρ = bulk density, kg/m^3
σ = surface tension, N/m
τ_a = acoustic time, s
τ_r = droplet-residence time, s
τ_v = velocity slip time, s
ϕ = phase angle, rad
ω = acoustic frequency, rad/s

Subscripts
a = air
f = fuel vapor
i = initial value
l = liquid
v = fuel vapor/air mixture at droplet surface
0 = steady-state solution

Superscript
$'$ = perturbation

Received Dec. 20, 1993; revision received Oct. 24, 1994; accepted for publication March 14, 1995.

*Graduate Student, Department of Aeronautical and Astronautical Engineering; currently Engineer, Mechanical Engineering Division, Northrop Grumman Corporation, 600 Hicks Road, M/S M-5000, Rolling Meadows, IL 60008-1098. Member AIAA.

†Professor, Department of Mathematics; currently Professor, Department of Aeronautical and Astronautical Engineering, University of Illinois, 104 South Wright Street, Urbana, IL 61801-2935. Member AIAA.

Introduction

INSTABILITIES in gas turbine combustion chambers have been studied for years in an effort to improve efficiency and performance and to minimize failure. One specific form of combustion instability consists of audible, high-amplitude, low-frequency pressure oscillations ("groaning") associated with the gas turbine combustion process. An underlying feature of these oscillations is a coupling between standing acoustic waves and unsteady heat-release fluctuations. This coupling can lead to a net energy gain in the system resulting in an increase in the oscillations, which will grow until limited by dissipative mechanisms such as viscous losses.[1] Groaning has been identified as occurring at subidle and near-idle conditions in the frequency range of 50–500 Hz.[2] Investigators such as Mehta et al.,[2] Kenworthy et al.,[3] and Vandsburger et al.,[4] have loosely correlated groaning with fuel volatility (i.e., the speed with which the fuel evaporates), and this depends on the size of the drops exiting the atomizer and the fuel evaporation characteristics. Kenworthy et al.[3] have identified these pressure oscillations as the cause of compressor stall, increased start-times, objectionable noise, and, in some instances, hardware failure.

High-temperature airstream pressure oscillations inside a gas turbine combustion chamber are associated with a variety of features inherent in these systems. Oscillating flowfields can be caused by the shedding of vortices from swirl cups and dilution holes located in the combustor,[5,6] the presence of mixing layers within the flow, and flow separation (or recirculation) zones at hardware component corners.[2] A fluctuating heat release partially in phase with this oscillatory flowfield

can sustain or enhance the pressure oscillations by feeding energy into them.[7]

Understanding the causes of unsteady heat release fluctuations will help investigators determine what type of modifications may be necessary to minimize the instabilities. Here we shall examine the slip mechanism identified in earlier works as a source of instability in premixed flames supported by particle/air mixtures.[8,9] Whereas in the earlier work the condensed phase is uniformly dispersed in the unbounded fresh mixture, here it is injected into the air carrier at a finite location. More precisely, the present work is concerned with premixed combustion in which the fuel is injected as liquid drops that evaporate to form gaseous fuel that mixes with the carrier stream of air upstream of the flame.

For the oscillations of interest, the inverse frequency defines a characteristic acoustic time of roughly 1 ms. A second time scale for the configuration is defined by how quickly the speed of the drops can respond to changes in the gas speed, a slip, or lag time. For the 80–100-μm drops of Ref. 2, this slip time is in the neighborhood of 1–10 ms. Consequently, when the multiphase mixture is perturbed by an acoustic wave, the condensed-phase stream will not be in phase with the gaseous stream. This can lead to fluctuations in the mixture flux fraction entering the combustion zone and the fluctuations in the burning strength that are generated can, in turn, generate acoustic signals. Provided the pressure fluctuations and the heat release fluctuations are in phase during a cycle (in the mean), an acoustic instability can be generated.

The details of this process can be complicated in the context of gas turbines. We are therefore of the opinion that it is useful to examine relatively simple idealized combustion configurations in which the interplay of the various physical processes can be explored in some detail with the hope of extracting general principles of value.

Model

Consider Fig. 1. At $x = 0$ fuel drops are uniformly injected into a uniform flow of air. The air is assumed sufficiently hot that the drops evaporate over a physically sensible length scale (~0.2 m) and evaporation is complete at $x = x_e$. The assumption of complete evaporation prior to the combustion zone is not without interest in view of the work being conducted in "premix-prevaporize" combustion chambers designed to diminish pollutant formation (Ref. 10, p. 16). An earlier, tentative discussion,[11] assumed, for simplicity, that the drops are injected at the gas speed U, but in real sprays the injection speed is much greater than that of the gas. This imparts a drag force on the drops that varies as the drops evaporate.

Superimposed on the flowfield is a standing acoustic wave that we anticipate, by analogy with Refs. 8 and 9, will generate fluctuations in the mixture flux fraction entering the combustion zone.

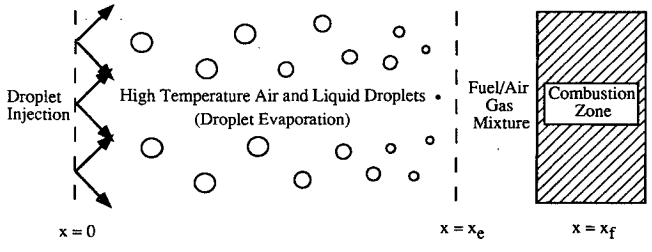

Fig. 1 Fuel spray model. The spray is injected at $x = 0$ into a uniform flow of gas of speed U. Evaporation is complete at $x = x_e$ and combustion occurs in some zone centered on $x = x_f$. In the steady state the mixture strength is uniform downstream of x_e, but in the presence of a standing acoustic wave it is perturbed. The magnitude of the perturbations depends on the drop slip time that is controlled, among other things, by the drop size.

Time Scales

Three time scales play important roles in the combustion system: 1) the acoustic time, τ_a; 2) the slip time, τ_v; and 3) the droplet-residence time, τ_r. The acoustic time is proportional to the inverse of ω, and for frequencies between 50–500 Hz, τ_a is of the order of milliseconds. As noted in Ref. 12, the only significant impact that the acoustic wave has on the drop environment is to the imposed velocity field. τ_v is a measure of the time required for droplet velocities to respond to these changes. It changes as the drop evaporates, and we calculate these changes, but a representative constant value can be defined for the purpose of the present comparisons. Using the discussion on slip times given by Marble,[13] and drag coefficient adjustments stated in Ref. 12, the representative velocity slip times are also on the order of milliseconds. A third time scale is τ_r, the evaporation time. Using Ref. 10, pp. 60–70 as a guide, droplet evaporation times are also on the order of τ_a and τ_v.

Thus, we are concerned with the situation for which all of the time scales are comparable. The acoustic and slip times must be comparable if the droplet is going to react to changes in the flowfield. For $\tau_v \gg \tau_a$, the droplets will travel through the evaporation zone unaffected by the acoustic wave, and for $\tau_v \ll \tau_a$, the droplets will react almost instantaneously to the changes and no lag will be perceived. In addition, $\tau_r \geq \tau_v$ will permit the droplets time to react to changes in the flowfield before evaporation is complete.

Selection of Test Conditions

In selecting the test conditions to use in the model, the fuel droplet sizes are calculated using the data presented by Mehta et al.[2,7,14] Since these authors performed the acoustic instability experiments using sections of actual flight hardware, realistic variations between the drop sizes of three fuels (JP-4, JP-5, and D-2) injected from a commercial atomizer are realized. With some exceptions, the airflow conditions are adjusted from the experiments to represent a premix–prevaporize combustion chamber (i.e., high inlet air temperature).

Mehta et al.[2,7] performed a variety of experiments with varying degrees of inlet temperature, inlet pressure, inlet air mass flow rate, and fuel/air ratio. Reference 7 describes the more recent published results; therefore, the air properties used in computing the droplet sizes of the JP-4 (gasoline-based), JP-5 (kerosene-based), and D-2 (diesel) fuels, are extracted from that source. These properties include an inlet air temperature and pressure of 392 K and 0.226 MPa, respectively, and a total inlet air mass flow rate of 0.726 kg/s. The tests were conducted in a 90-deg section of a commercial combustion chamber containing five swirl cups. Since the inlet air mass flow rate was divided among five cups, the flow rate of air reaching each cup was one-fifth the total or 0.145 kg/s. A schematic of the hybrid atomizer used in the experiments of Refs. 2 and 7 is shown in Fig. 4 of Ref. 14. From this figure, the airstream is shown to be divided among a primary and secondary channel. Approximately 70% of the inlet air mass flow rate passing through each atomizer is diverted through the primary flow channel; therefore, approximately 0.102 kg/s of air mass flow acts as the primary atomizing airstream.

For most engineering purposes, classifying a spray as being composed of droplets of identical size is satisfactory. There are several different ways to express mean drop size and one of the most popular is *SMD*. *SMD* represents the diameter of a droplet with a volume to surface area ratio equal to that of the entire spray (Ref. 15, pp. 90–91). Since hybrid atomizers are a derivative of prefilming atomizers (Ref. 15, p. 140), empirical relations developed for prefilming air blast atomizers will provide a satisfactory approximation for the *SMD* of the droplets injected in the experiments of Refs. 2

and 7. From experimental data, Rizkalla and Lefebvre deduced the following empirical equation[16]:

$$SMD = 3.33 \times 10^{-3} \frac{(\sigma_l W_l D_p)^{0.5}}{W_a U_i}(1 + FAR) + 13.0 \times 10^{-3}\left(\frac{\mu_l^2}{\sigma_l W_l}\right)^{0.425} D_p^{0.575}(1 + FAR)^2 \quad (1)$$

In Refs. 2 and 7 the fuel was tested at 293 K and at atmospheric pressure; therefore, the fuel properties of surface tension (σ_l), viscosity (μ_l), and density (W_l) for the three fuels may be identified from Refs. 17–20 and are shown in Table 1. As defined by Mehta et al.,[2] *FAR* expressed in their experiments represented an "overall volume average fuel-air ratio deduced from global fuel and air mass balances." This value was varied between 0.010–0.040. D_p stands for the prefilmer diameter, which represents the i.d. of the atomizer venturi (see Fig. 4 from Ref. 14) and measures 0.0584 m. The air velocity U_i expressed in Eq. (1) represents the impinging velocity on the fuel stream. This value can be approximated from the results of Ref. 14 using Fig. 7 from that source. As calculated,[21] the resulting air velocity impinging on the fuel stream is approximately 21 m/s. With all necessary information found, Eq. (1) can be solved for the *SMD* of the fuels (Table 2).

In determining the fuel and air properties to use in the model, it is assumed that the droplets completely evaporate before reaching the reaction zone. This assumption leads to the selection of an air temperature higher than the 392 K temperature used in Ref. 7. To ensure complete fuel evaporation, the selected air temperature and pressure are 1000 K and 0.225 MPa, respectively. An airstream velocity of 10 m/s is selected to keep the droplet evaporation distance to around 0.20 m (a physically sensible length scale).

The procedure described by Chin and Lefebvre[22] and Lefebvre[15] pp. 309–326 is implemented to determine the necessary fuel properties such as steady-state temperature, specific heat, density, latent heat of vaporization, viscosity, and thermal conductivity. As described in Ref. 22, a "steady state" rarely occurs during a droplet lifetime during evaporation or combustion, but for most light distillate fuels, a quasisteady gas phase containing the primary features of mass and thermal diffusion will still allow estimation of evaporation rates and lifetimes to be determined within a reasonable level of accuracy. In the context of Ref. 22, steady state represents the droplet evaporation stage when the droplet has stabilized at its wet-bulb temperature and all of the heat reaching the droplet surface provides the latent heat of vaporization.

Due to the complex nature of the flowfields inside and above the fuel droplets, it is difficult to develop a straightforward procedure to calculate necessary fuel properties. As a matter of fact, in many droplet evaporation calculations, the properties of the fuel vapor/air mixture existing above the droplet surface are also required. Chin and Lefebvre[22] found, by using a simplified droplet evaporation model, that they could still obtain results that are in good agreement with published experimental results. In determining the steady-state fuel evaporation temperature T_l, Chin and Lefebvre utilized the classical droplet evaporation model of Spalding.[23] The classical Spalding model assumes a spherically symmetric quasisteady state (since the relative densities of air and fuel differ greatly) with the droplet of uniform and constant temperature and uniform concentration. Lefebvre (Ref. 15, p. 328) has argued that forced convection does not alter the steady-state evaporation temperature and we shall fix T_l at the value found using the Chin and Lefebvre analysis. A summary of the resulting properties used in the present model is listed in Table 3. In addition to the results in Table 3, an initial Reynolds number, defined as[12]

$$Re_d = (2r_l)u_r W_a/\mu_v \quad (2)$$

Table 1 Fuel properties used in droplet size calculations[a]

Property	JP-4	JP-5	D-2
σ_l, N/m	2.18×10^{-2}	2.37×10^{-2}	3.03×10^{-2}
μ_l, kg/m-s	0.72×10^{-3}	1.34×10^{-3}	3.82×10^{-3}
W_l, kg/m^3	760.0	815.0	850.0

[a]At 293 K and 1 atm.

Table 2 *SMD* of tested fuels

Fuel	*SMD*, μm
JP-4	80
JP-5	90
D-2	105

Table 3 Summary of air, liquid droplet, and fuel vapor/air environment properties

Property	JP-4	JP-5	D-2
T_l, K	422.0	490.0	526.0
W_l, kg/m^3	449.6	493.4	506.8
C_{pv}, kJ/kg-K	1.97	2.01	2.04
k_v, kW/m-K	4.34×10^{-5}	4.13×10^{-5}	3.94×10^{-5}
L_v, kJ/kg	290.8	269.3	259.2
μ_v, kg/m-s	2.13×10^{-5}	2.39×10^{-5}	2.49×10^{-5}
T_a, K		1000	
P_a, kPa		225	
W_a, kg/m^3		0.783	
U, m/s		10	

Table 4 Initial drop velocities[a]

Diameters	JP-4	JP-5	D-2
Different	95.0 m/s, 80 μm	94.5 m/s, 90 μm	85.5 m/s, 105 μm
Identical	95.0 m/s, 80 μm	105.0 m/s, 80 μm	109.0 m/s, 80 μm

[a]Re_d: 250.

of 250 is used for each fuel. r_l represents the droplet radius and u_r represents the relative velocity between the fuel drops and air ($=u_l - U$). The choice of Re_d at $x = 0$ was selected to keep the evaporation distance to the length scale of approximately 0.20 m. The resulting initial drop velocities for the drop diameters calculated earlier, and for equal drop diameters of 80 μm, are listed in Table 4.

Equations

The derivation of the governing equations describing a one-dimensional forced convection system with evaporation (Fig. 1) is detailed in Refs. 12 and 21 and these equations appear next.

As noted, the evaporation rate is assumed to depend on the instantaneous state of the drop and its environment, without lag. The role that lag of this nature can play in driving an instability in situations where the drop is immersed in the fire has been extensively discussed, but it is a characteristic of the mechanism described here that it does not require this ingredient. The equations are

$$\frac{\partial \rho_l}{\partial t} + \frac{\partial}{\partial x}(\rho_l u_l) = -f, \qquad \rho_a\left(\frac{\partial Y_f}{\partial t} + u_a \frac{\partial Y_f}{\partial x}\right) = f \quad (3)$$

$$f = -\frac{3\rho_l}{r_l}\left(\frac{\partial r_l}{\partial t} + u_l \frac{\partial r_l}{\partial x}\right) \quad (4)$$

$$\frac{\partial r_l}{\partial t} + u_l \frac{\partial r_l}{\partial x} = \frac{A_1}{r_l}\{1 + A_2[r_l(u_l - u_a)]^{1/2}\} \quad (5)$$

$$\frac{\partial u_l}{\partial t} + u_l \frac{\partial u_l}{\partial x} = A_3 \frac{(u_l - u_a)}{r_l^2}\{1 + A_4[r_l(u_l - u_a)]^{2/3}\} \quad (6)$$

where

$$A_1 = -\frac{k_v}{W_l C_{pv}} \mathcal{N}\left[1 + \frac{C_{pv}(T_a - T_l)}{L_v}\right], \qquad A_2 = 0.30 Pr_v^{0.33}\sqrt{\frac{2W_a}{\mu_v}} \quad (7)$$

$$A_3 = -\frac{9\mu_v}{2W_l\left[1 + \frac{C_{pv}(T_a - T_l)}{L_v}\right]}, \qquad A_4 = \frac{1}{6}\left(\frac{2W_a}{\mu_v}\right)^{2/3} \quad (8)$$

Here, f is an evaporation term responsible for a decrease in ρ_l, an increase in Y_f, and a decrease in r_l. f is defined by a classical static term A_1 modified by convection (the term in A_2), see Ref. 15. Equation (6) is an extension of Newton's third law for the liquid phase, corresponding to a drag coefficient (Ref. 15, pp. 304, 305):

$$C_D = \frac{\frac{24}{Re_d}\left(1 + \frac{1}{6}Re_d^{2/3}\right)}{\left[1 + \frac{C_{pv}(T_a - T_l)}{L_v}\right]} \quad (9)$$

We assume, for simplicity, that the fuel loading is small so that the gas flow is not affected by the presence of the drops. This flow is then characterized by a uniform flow of speed U together with an acoustic disturbance for which

$$u_a' = \varepsilon U e^{i\omega t}\cos[(\omega x/c) + \phi] \quad (10)$$

for some ϕ. ε is a small parameter that characterizes the amplitude of the acoustic wave. Since $\omega x_e/U$ is assumed to be O(1) (recall the discussion of time scales), and the Mach number is small, this equation can be replaced by

$$u_a' = \varepsilon U e^{i\omega t}\cos(\phi) \quad (11)$$

Note that temperature fluctuations are of the order $MT_a u_a'/U$, and so are negligible. Pressure fluctuations are also small (order $MP_a u_a'/U$), but the pressure does not appear in Eqs. (3–9) anyway.

Unperturbed Solution

If we set $u_a' = 0$, so that $u_a = U$, the unperturbed solution is readily constructed by numerical means. This contrasts with the simplified model of Ref. 11 in which an analytical description is possible. The unperturbed solution, calculated numerically for JP-4 fuel, appears in Fig. 2, where we have made the identity $x \to s$. These profiles display a square-root singularity at s_e, the point at which evaporation is complete, so that, for example , $r_l \propto \sqrt{s_e - s}$ in the neighborhood of s_e. This singularity leads to difficulties in the calculation of perturbation quantities.

Perturbations

To describe the perturbations generated by the acoustic wave we set $u_a = U + u_a'$ and linearize the equations about the unperturbed state, with the replacement $\partial/\partial t \to i\omega$. In calculating perturbations of a function $f(x, \varepsilon)$ for small ε, different strategies are possible. The conventional approach is to describe the perturbed solution by adding a perturbation

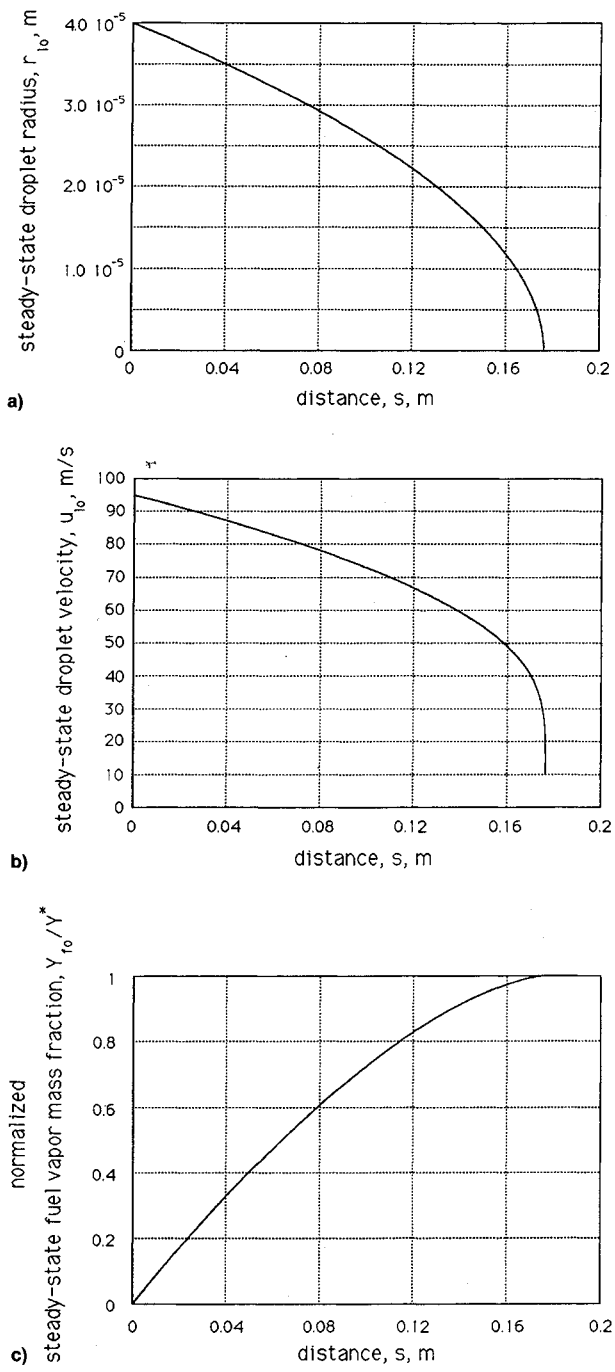

Fig. 2 Steady-state solution (during droplet evaporation) (JP-4 fuel only), $\{Y^* = \rho_{l_0}[(0)u_{l_0}(0)/\rho_a U]\}$. Steady-state a) droplet radius, b) droplet velocity, and c) fuel vapor mass fraction.

$f'(x, \varepsilon)$ to the unperturbed solution $f_0(x) \equiv f(x, 0)$. In this scenario, x is fixed and we calculate the vertical displacement of the graph of f, namely $f(x, \varepsilon) - f_0(x) \equiv f'$. An alternative strategy is to fix f and describe the horizontal displacement of the graph so that $f(x, \varepsilon) = f_0(x + x')$ for some perturbation $x'(x, \varepsilon)$. The first choice (a regular perturbation analysis) does not suffice for our problem. It leads to unacceptable singularities at $x = x_e$ because it fails to account for the displacement of the point at which evaporation is complete. To account for this it is necessary to use the second choice, Lighthill's method of coordinate stretching, developed to describe the far-field Mach wave steepening responsible for the sonic boom. Reference 24 contains a delightfully clear description of the strategy. In practice, a combination (nonunique) of the two strategies is usually adopted (i.e., the description contains

both f' and x' terms) and the only important constraint is that unacceptable singularities be eliminated. Thus, we seek perturbations of any fluid variable Φ in the form

$$\Phi \sim \Phi_0(s) + \varepsilon e^{i\omega t}\Phi_1(s) + \cdots \tag{12}$$

where Φ_0 is the steady state and

$$x \sim s + \varepsilon e^{i\omega t}x_1(s) + \cdots, \qquad x_1(0) = 0 \tag{13}$$

To leading order $x = s$ so that unperturbed formulas are still valid after the substitution $x \to s$, accounting for the choice in Fig. 2. A proper (but nonunique) choice of the stretching function $x_1(s)$ follows from an examination of the perturbations. The fundamental rule is that perturbations should be no more singular than the unperturbed solution. The choice $x_1(s) \equiv 0$, for example, leads to a solution for which $r_f' \propto 1/\sqrt{s_e - s}$ in the neighborhood of s_e, and this is not acceptable. A simple choice of $x_1(s)$ that works is one for which

$$r_f' \equiv 0 \tag{14}$$

so that the drop-size perturbations are accounted for purely by a nonuniform stretching of the steady solution, and that is the one that we have adopted. The perturbation equations are easily integrated using a fourth-order Runge–Kutta scheme with initial conditions:

$$u_l'(0) = \rho_l'(0) = Y_f'(0) = 0 \tag{15}$$

Plots of the maximum fuel vapor mass fraction perturbation against frequency, using the data of Tables 2 and 3, are presented in Fig. 3. To avoid an acoustic node at the injector location, an arbitrary ϕ of 1 rad is used in all of the plots so that $\cos\phi = 0.54$. The frequency range for the plots of this article is from 30 to 500 Hz (groaning is identified as occurring between 50–500 Hz). Note that the mass flux of gas is

$$\rho_a(U + u_a') \tag{16a}$$

and the mass flux of liquid at the injection point is

$$\rho_{l_0}(0)u_{l_0}(0) \tag{16b}$$

so that the mass flux fraction of fuel at $x = 0$ is

$$Y^*(1 - \varepsilon\cos\phi\varepsilon^{i\omega t} \ldots), \quad Y^* \equiv \frac{\rho_{l_0}(0)u_{l_0}(0)}{\rho_a U} \tag{17}$$

It follows that in the limit of vanishing frequency the amplitude of the mass fraction perturbation for $x > x_e$ is $\varepsilon\cos\phi Y^*$. (Note that this conclusion is independent of the spray characteristics apart from those appearing in the numerator of Y^*.) This is of no practical concern since it does not fluctuate and so cannot generate a fluctuating heat output downstream of x_e to couple with the acoustic wave. As the frequency is increased, Y_f' decreases quite sharply, but at moderate, physically realistic frequencies the amplitude is still quite significant and is a potential driver of instability provided Rayleigh's criterion is satisfied within the combustion zone and provided the wave can fit within the apparatus. (It is these latter considerations that would "select" a frequency from the range of frequencies that the present analysis predicts will give significant fluctuations of Y_f'.) The quantity $\varepsilon(Y_f'/\varepsilon Y^*)$ is the ratio of the perturbation rate of heat generation to the unperturbed rate, and the values shown in Fig. 3 would be approximately doubled if the least desirable phase angle ($\phi = 0$) was chosen, so that these are substantial fluctuations at low frequencies.

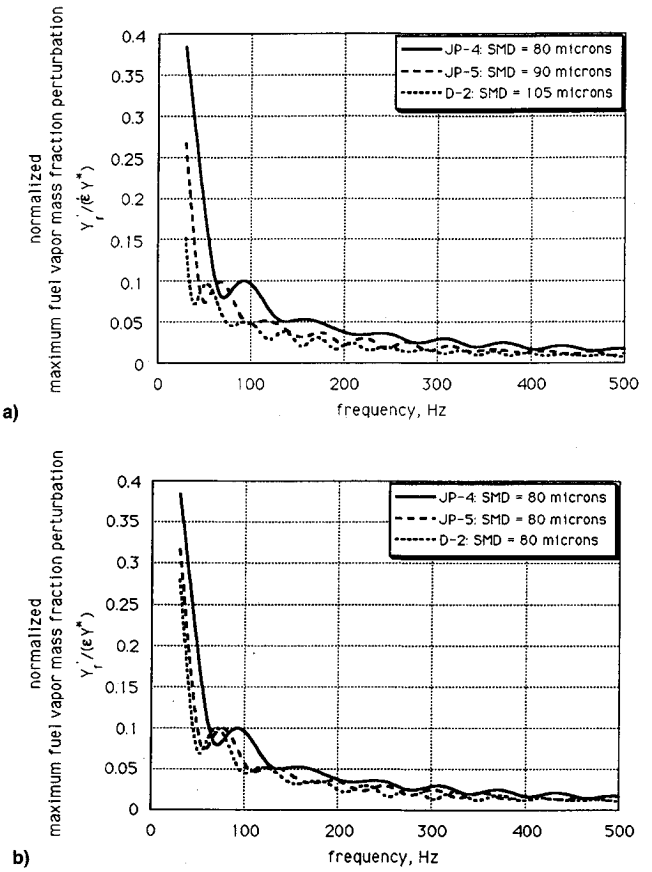

Fig. 3 Variation of maximum fuel vapor mass fraction perturbation with frequency (initial droplet size effect) $\{Y^* = e^{i\omega t}[\rho_{l_0}(0)u_{l_0}(0)/\rho_a U]\}$: a) different and b) identical *SMD*s at injection.

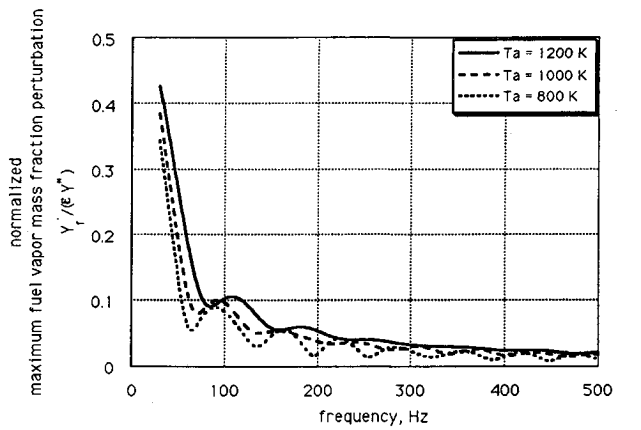

Fig. 4 Variation of maximum fuel vapor mass fraction perturbation with frequency (air temperature effect) (JP-4 fuel), $\{Y^* = e^{i\omega t}[\rho_{l_0}(0)u_{l_0}(0)/\rho_a U]\}$.

Experiments at the University of Marseille on premixed flames propagating into droplet/air mixtures (the configuration studied theoretically in Ref. 9) suggest that in that context, fluctuations in mixture strength generated by acoustic waves can be a powerful driver of instabilities.[25] Note that for a wide range of frequencies the magnitude of the driving effect increases with the order D-2, JP-5, and JP-4, which is consistent with the correlations with volatility observed in Refs. 2–4.

In addition to examining how the droplet sizes affect the perturbations, we can examine the impact of changes in inlet air temperature, steady-state air velocity, and initial Reynolds number on the measured fluctuations. Figure 4 shows the

effect of inlet air temperature for JP-4 fuel. In this analysis, the fuel properties are re-evaluated with the initial Re_d maintained at 250. The changes result in steady-state fuel droplet temperatures of 411, 422, and 428 K, for inlet air temperatures of 800, 1000, and 1200 K, respectively (with corresponding fuel property changes), and injected droplet velocities of 73.5, 95, and 119 m/s, respectively. Increasing the air temperature increases the fuel evaporation rate. The results show that an increased fuel evaporation rate (related to volatility) increases the fuel vapor mass fraction fluctuations.

Figure 5 shows the effect of the steady-state air velocity for JP-4 fuel, with the initial Reynolds number maintained at 250. To maintain an initial Re_d of 250, increasing the air velocity from 10, to 15, and to 20 m/s, requires an increase in the injected droplet velocity from 95, to 100, and to 105 m/s, respectively. An identical initial Reynolds number results in identical initial relative velocities between the three. Higher air velocities are found to increase the maximum perturbations.

Figure 6 shows the effect of different initial Reynolds numbers for JP-4 fuel, which relates to different initial relative velocities between the air and fuel. Using the fuel and air properties of Table 3, a steady-state air velocity of 10 m/s, and droplet diameter of 80 μm, a change in the initial Reynolds number from 150, to 250, to 350, results in initial relative velocities of 51, 85, and 119 m/s, respectively, with corresponding injected droplet velocities of 61, 95, and 129 m/s. The results show that at higher initial Reynolds numbers, the maximum perturbations decrease, which relates to the fact

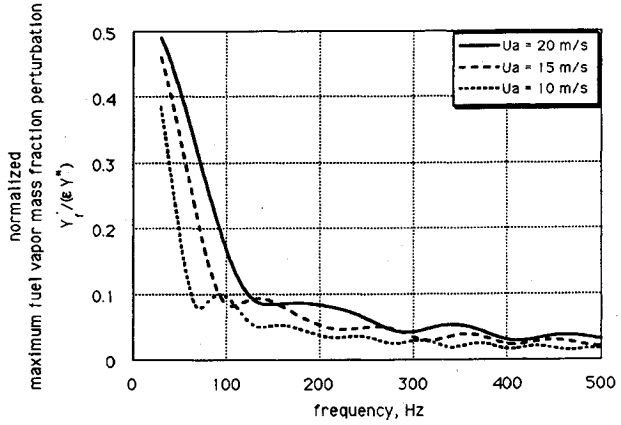

Fig. 5 Variation of maximum fuel vapor mass fraction perturbation with frequency (air velocity effect) (JP-4 fuel), $\{Y^* = e^{i\omega t}[\rho_{l_0}(0)u_{l_0}(0)/\rho_a U]\}$.

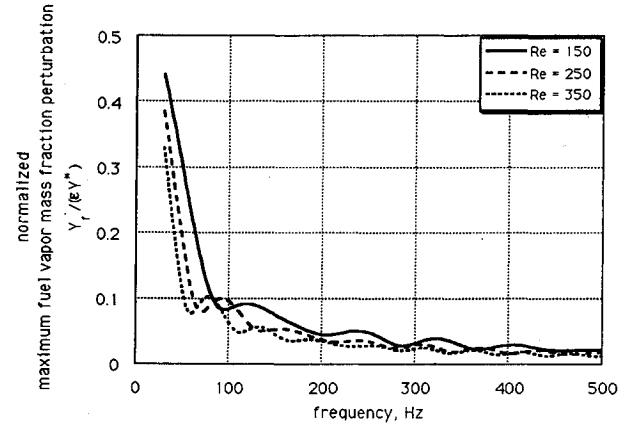

Fig. 6 Variation of maximum fuel vapor mass fraction perturbation with frequency (initial Reynolds number effect) (JP-4 fuel), $\{Y^* = e^{i\omega t}[\rho_{l_0}(0)u_{l_0}(0)/\rho_a U]\}$.

that, as the lag time is increased, the drops are not given enough time to react to airstream changes before they completely evaporate.

Concluding Remarks

We have shown that when a spray is injected into a gas flow (in the context of gas turbines) and an acoustic wave is present, slip or lag between the velocity of the gas and that of the condensed phase can lead to significant fluctuations in the mass flux fraction of fuel vapor entering the combustion zone. These fluctuations will generate fluctuations in the heat output, and if these are sufficiently in phase with the pressure fluctuations, they could drive the acoustic wave, implying instability. For the parameter values that we have chosen this effect will be noticeable at low frequencies.

The magnitude of the effect can be ordered with respect to properties such as volatility over finite intervals of frequency. This kind of behavior is consistent with experimental observations of groaning in gas turbines.

One of the limitations of our analysis is that it is restricted to situations in which evaporation is complete before the combustion zone is reached. This represents a limiting situation, amenable to a relatively straightforward analysis. (A different simple situation is examined in Refs. 8 and 11 in which the phase conversion occurs in the preheat zone of what is, fundamentally, a classical deflagration wave–slip leads to fluctuations in the fuel mass flux fraction at a thin reaction zone located at the downstream boundary of the preheat zone.) We can see that there will be an effect in the general case from the following argument.

The fuel/air mass flux ratio, in the small loading limit, is

$$MFR = (\rho_l u_l/\rho_a u_a) + Y_f \tag{18}$$

Thus, the unperturbed flux ratio is

$$MFR_0 \equiv \frac{\rho_{l_0} u_{l_0}}{\rho_a U} + Y_{f_0} = \frac{\rho_{l_0}(0)u_{l_0}(0)}{\rho_a U} \tag{19}$$

The perturbation is given by the formula

$$MFR' e^{-i\omega t}\frac{\rho_a U}{\rho_{l_0}(0)u_{l_0}(0)} = \frac{(\rho_l u_l)' e^{-i\omega t}}{\rho_{l_0}(0)u_{l_0}(0)} - \frac{\rho_{l_0}u_{l_0}e^{-i\omega t}}{\rho_{l_0}(0)u_{l_0}(0)}\frac{u'}{U} + \frac{\rho_a U Y_f' e^{-i\omega t}}{\rho_{l_0}(0)u_{l_0}(0)} \tag{20}$$

The amplitude of this expression (divided by ε) is plotted as a function of (s/s_e) in Fig. 7 for the data of Fig. 3a and a frequency of 50 Hz. At $s = s_e$, where $\rho_l = 0$, we recover points plotted in Fig. 3a.

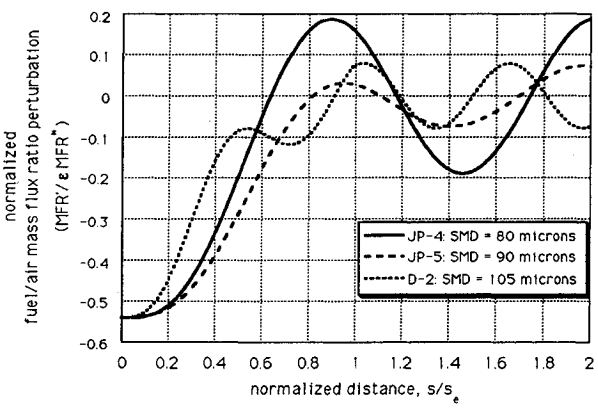

Fig. 7 Variation of fuel/air mass flux ratio perturbation with distance (frequency = 50 Hz), $\{MFR^* = e^{i\omega t}[\rho_{l_0}(0)u_{l_0}(0)/\rho_a U]\}$.

An important point to notice about this quantity is that it does not vanish at the injection point, and we could introduce a fire anywhere downstream of the injection point and still have significant variations in the mass flux ratio entering the fire. As pointed out in Ref. 11, this is true even for very small drops, when the slip time is small. Decreasing the slip time decreases the distance over which the drop speed adjusts to the gas speed, but does not eliminate the fluctuations in *MFR* that are generated in this adjustment zone.

One of the assumptions that we have been forced to make in order for the analysis to be tractable is that the drops are all of the same size. In practice there will be a distribution of sizes and the different size drops will respond in different ways to the acoustic wave. As noted following Eq. (17), this will not affect the mass fraction perturbation in the limit of vanishing frequency, and so it is the extent of the drop-off in response with increasing frequency that is of interest. Too sharp a drop-off so that the response is small for wavelengths short enough to fit within the device and the tendency to instability could be overwhelmed by acoustic energy losses (including those due to the drag of the drops). At the present time we do not know what effect a size distribution will have in this connection. The question arises in premixed flames, but has not been answered there either.[9] As noted earlier, the instability has been observed in premixed flames.

Acknowledgments

This work was supported by AFOSR and the NASA Lewis Research Center. We are grateful to Lee Dodge, who suggested that the mechanism discussed in Ref. 8 could be responsible for gas turbine groaning, and to J. Adler, whose question at the 21st Symposium[8] further fueled our interest in this possibility. D. Lozinski, J. M. Mehta, and J. E. Peters provided valuable advice, and for this we are grateful. In addition, L. Brandolino of Amoco Oil Research provided invaluable help in the acquisition of fuel property information.

References

[1]Rayleigh, J. W. S., *The Theory of Sound*, Vol. 2, Dover, New York, 1945, pp. 224–235.

[2]Mehta, J. M., Mungur, P., Dodds, W., Bahr, D. W., and Clouser, S., "Fuel Effects on Gas Turbine Combustor Dynamics," AIAA Paper 90-1957, July 1990.

[3]Kenworthy, M. J., Bahr, D. W., Mungur, P., Burrus, D. L., Mehta, J. M., and Cifone, A. J., "Dynamic Instability Characteristics of Aircraft Turbine Engine Combustors," *AGARD Conference Proceedings 450 on Combustion Instabilities in Liquid-Fueled Propulsion Systems*, AGARD CP-450, 1989, Sec. 4, pp. 1–13.

[4]Vandsburger, U., McManus, K., and Bowman, C., "Effects of Fuel Spray Vaporization on the Stability Characteristics of a Dump Combustor," AIAA Paper 89-2436, July 1989.

[5]Jou, W.-H., and Menon, S., "Numerical Simulation of the Vortex-Acoustic Wave Interaction in a Dump Combustor," AIAA Paper 86-0002, Jan. 1986.

[6]Sterling, J. D., and Zukoski, E. E., "Longitudinal Mode Combustion Instabilities in a Dump Combustor," AIAA Paper 87-0220, Jan. 1987.

[7]Mehta, J. M., Mungur, P., Dodds, W., Bahr, D. W., and Clouser, S., "Thermoacoustics of Unsteady Combustion," AIAA Paper 90-3928, Oct. 1990.

[8]Buckmaster, J., and Clavin, P., "An Acoustic-Instability Theory for Particle-Cloud Flames," *Proceedings of the 24th Symposium (International) on Combustion*, The Combustion Inst., Pittsburgh, PA, 1992, pp. 29–36.

[9]Clavin, P., and Sun, J., "Theory of Acoustic Instabilities of Planar Flames Propagating in Sprays or Particle-Laden Gases," *Combustion Science and Technology*, Vol. 78, Nos. 4–6, 1991, pp. 265–288.

[10]Lefebvre, A. H., *Gas Turbine Combustion*, Hemisphere, New York, 1983, pp. 16, 60–70.

[11]Lee, C. J., Buckmaster, J., and DiCicco, M., "Intrinsic and Acoustic Instabilities in Flames Fueled by Multiphase Mixtures," *Combustion Science and Technology*, Vol. 98, 1994, pp. 161–184.

[12]DiCicco, M., and Buckmaster, J., "Acoustic Instabilities Driven by Slip Between a Condensed Phase and the Gas Phase in Combustion Systems," AIAA Paper 94-0103, Jan. 1994.

[13]Marble, F. E., "Dynamics of Dusty Gases," *Annual Review of Fluid Mechanics*, Vol. 2, 1970, pp. 397–446.

[14]Mehta, J. M., Shin, H.-W., and Wisler, D. C., "Mean Velocity and Turbulent Flow-Field Characteristics Inside an Advanced Combustor Swirl Cup," AIAA Paper 89-0215, Jan. 1989.

[15]Lefebvre, A. H., *Atomization and Sprays*, Hemisphere, New York, 1989, pp. 90, 91, 140, 304–326, 344–351.

[16]Lefebvre, A. H., "Atomization of Alternative Fuels," *Combustion and Fuels in Gas Turbine Engines*, AGARD CP-422, 1988, pp. 3: 1–13.

[17]*Handbook of Aviation Fuel Properties*, Coordinating Research Council, Inc., CRC Rept. 530, Atlanta, GA, 1983, pp. 22, 34, 38.

[18]*A.S.T.M. Tentative Viscosity-Temperature Charts for Liquid Petroleum Products*, American Society for Testing Materials, Chart D: Kinematic Viscosity, Low Range, Philadelphia, PA, 1992.

[19]"Surface Tension of Pure Hydrocarbons," *Technical Data Book*, Amoco Oil Co., Naperville, IL, 1982, Fig. 10A1.5.

[20]"Densities of Liquid Petroleum Fractions at Low Pressures," *Technical Data Book*, Amoco Oil Co., Naperville, IL, 1983, Fig. 6A3.5.

[21]DiCicco, M., "Acoustic Instabilities Driven by Slip Between a Condensed Phase and the Gas Phase in Combustion Systems," M.S. Thesis, University of Illinois, Urbana, IL, 1994.

[22]Chin, J. S., and Lefebvre, A. H., "Steady-State Evaporation Characteristics of Hydrocarbon Fuel Drops," *AIAA Journal*, Vol. 21, No. 10, 1983, pp. 1437–1443.

[23]Spalding, D. B., "The Combustion of Liquid Fuels," *Proceedings of the 4th Symposium (International) on Combustion*, The Combustion Inst., Pittsburgh, PA, 1952, pp. 847–864.

[24]Van Dyke, M., *Perturbation Methods in Fluid Mechanics*, Parabolic Press, Stanford, CA, 1975, pp. 99–120.

[25]Clavin, P., private communication, 1993.